Tunable Photonic Crystals Containing Graphene and PEDOT:PSS Polymer in THz

A. Gharaati and M. Ranjbar*

Department of Physics, Payame Noor University, Tehran 19395-4697, Iran

Received: 28.08.2021 & Accepted: 08.11.2021

Doi: 10.12693/APhysPolA.140.433 *e-mail: marzieh.ranjbar20@gmail.com

In this work, the optical properties of one-dimensional photonic crystal structures which contain two dielectrics combined with graphene layers, and Poly (3,4-ethylenedioxythiophene):poly (4-styrenesulfonate) (PEDOT:PSS), are reported by using the transfer matrix method. For this purpose, an ideal crystal composed of an alternating layer of SiO_2 and Si is considered. The permittivity of the conductive polymer PEDOT:PSS is calculated as a function of the frequency from the Drude–Smith model. When PEDOT:PSS inserts as a defect layer in the two proposed structures with and without graphene layers, the resonant defect mode appears in prohibited region. Results show that the arrangement of graphene layers in the structures tunes the position and height of the resonance mode. The graphene chemical potential and the incident angle of the transverse electric wave also affects the tuning of the PBGs and resonant modes. Therefore, the proposed structures can be beneficial in the fabrication of the tunable low terahertz filters.

topics: photonic crystal, graphene, polymer PEDOT:PSS, terahertz frequency range

1. Introduction

Yablonovitch and John proposed the photonic crystals (PCs) concept in 1987 [1, 2]. Since then, researchers have tried to design and fabricate these periodic structures with a variety of materials. If the thickness of the PC layer changes or a layer with a different refractive index is added to the PC structure, a resonance mode appears in the prohibited region called PBG, where electromagnetic waves are not allowed to propagate in this range [3, 4]. Becasue of these special properties of PC, optical and optoelectronic devices like filters [5], waveguides [6], resonators [7], sensors, and biomedical sensors [8] have been built.

PEDOT:PSS polymer with high conductivity, thermal stability, and low cost can be a good candidate material in the terahertz (THz) region. Recently, the design of tunable devices in the THz range has been considered [9]. Different materials are used in the structure of photonic crystals, the permittivity of which can be adjusted by voltage, external magnetic field or temperature [10]. One of these materials is graphene with a two-dimensional honeycomb lattice structure and unique properties [11]. The change in the chemical potential of graphene depends on the external voltage gate, which is one of the tuning effective factors for the conductivity of the graphene surface [12].

In this work, SiO_2 and Si have been used as alternating layers in the proposed photonic crystal structures, by inserting the polymer defect layer and graphene layers in the proposed structures. The tenability, the dependency on the chemical potential of graphene sheets and the incident angle are explored. The position and height of the defect mode of the two proposed structures in terms of different chemical potentials are compared at three different angles.

2. Materials and methods

2.1. PC structure

In structures, dielectric layers A and B for SiO_2 and Si, respectively, with the dielectric permittivity ε_{SiO_2} and ε_{Si} are considered. As shown schematically in Fig. 1a, the ideal 1D photonic crystal of a structure $(AB)^N$ is composed of alternating layers SiO_2 and Si. In Fig. 1b, a conductive polymer PEDOT:PSS is added to the structure as a defect layer, and graphene monolayers are placed between each dielectric layer for tuning in structure b, $[(AGBG)^{N_1}]P[(GBGA)^{N_2}]$. Figure 1c illustrates the structure c, $[(GAB)^{N_1}G]P[G(BAG)^{N_2}]$. In this structure, two different dielectric layers are placed next to each other and sandwiched with graphene layers, then repeated alternately, after which the polymer PEDOT:PSS is placed in the structure as a defect mode. In this paper, Fig. 1a, Fig. 1b, and Fig. 1c will be referred to as ideal crystal, structure b, and structure c, respectively.

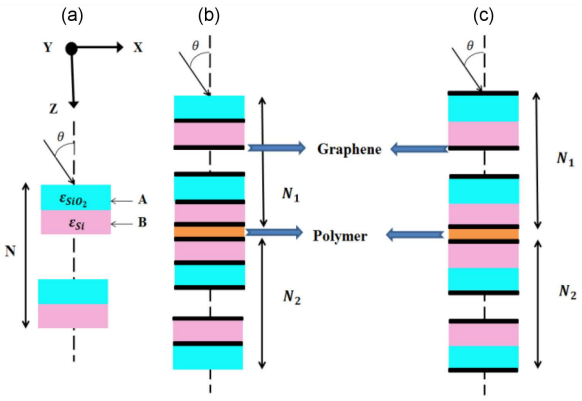

Fig. 1. The schematics of (a) ideal 1D photonic crystal and proposed defective structures with (b) $[(\mathrm{AGBG})^{N_1}]\mathrm{P}[(\mathrm{GBGA})^{N_2}]$, (c) $[(\mathrm{GAB})^{N_1}\mathrm{G}]\mathrm{P}[\mathrm{G}(\mathrm{BAG})^{N_2}]$ geometries.

Here, it is assumed that the PC is surrounded by air, and the incident wave has an angle θ with the Z-axis. Each layer of the PC structures is selected parallel to the XY plane so that the Z direction is normal to the structures.

2.2. Graphene

Graphene is a single layer of carbon atoms arranged in two-dimensional (2D) hexagonal lattice structures.

For a uniaxial graphene stripe in the X–Y plane, the permittivity tensor is given as [13, 14]

$$\varepsilon_{\mathrm{G}} = \begin{bmatrix} \varepsilon_{\mathrm{G},t} & 0 & 0 \\ 0 & \varepsilon_{\mathrm{G},t} & 0 \\ 0 & 0 & \varepsilon_{\mathrm{G},\perp} \end{bmatrix}, \tag{1}$$

where $\varepsilon_{G,t}$ and $\varepsilon_{\mathrm{G},\perp}$ are the tangential and normal components of graphene permittivity, respectively. It is necessary to state that the normal electric field cannot excite any current in the 2D graphene sheet. The normal permittivity component could be regarded as $\varepsilon_{\mathrm{G},\perp} = 1$. The tangential component depends on parameters such as angular frequency (ω), the permittivity of the vacuum (ε_0), the thickness of graphene layer (d_{G}), temperature, and the graphene chemical potential (μ_c) [13, 14]. The dependence is

$$\varepsilon_{\mathrm{G},t} = \varepsilon_{\mathrm{G},\perp} + \mathrm{i}\frac{\sigma(\omega)}{\varepsilon_0 \omega d_{\mathrm{G}}}. \tag{2}$$

From the Kubo formula, the surface conductivity of graphene is calculated from the sum of the intra-band and inter-band conductivity, which is presented by [14]

$$\sigma(\omega) = \sigma_{\mathrm{intra}} + \sigma_{\mathrm{inter}}, \tag{3}$$

where

$$\sigma_{\mathrm{intra}} = \mathrm{i}\frac{\mathrm{e}^2}{\pi\hbar}\frac{k_{\mathrm{B}}T}{(\omega + \mathrm{i}\Gamma)} \times \left[\frac{\mu_c}{k_{\mathrm{B}}T} + 2\ln\left(\mathrm{e}^{-\mu_c/k_{\mathrm{B}}T} + 1\right)\right], \tag{4}$$

and

$$\sigma_{\mathrm{inter}} = \mathrm{i}\frac{\mathrm{e}^2}{4\pi\hbar}\ln\left(\frac{2\mu_c - (\omega + \mathrm{i}\Gamma)}{2\mu_c + (\omega + \mathrm{i}\Gamma)}\right). \tag{5}$$

Here, e, k_{B}, T, $\hbar$, Γ, and μ_c are the charge of an electron, the Boltzmann constant, the Kelvin temperature, reduced Plank's constant, scattering rate, and chemical potential, respectively. In this work, transverse electric (TE) polarized waves are considered. The dispersion relation for the TE polarized wave, for an anisotropic graphene sheet, is determined by [13, 14]

$$k_x^2 + k_z^2 = \varepsilon_{\mathrm{G},t} k_0^2. \tag{6}$$

2.3. The PEDOT:PSS Polymer

Poly (3, 4-ethylenedioxythiophene):poly (4-styrenesulfonate) (PEDOT:PSS) is a good candidate for electro–optical devices in the terahertz region. High conductivity and environmental stability are features that make the PEDOT:PSS superior to other conductive polymers. The dielectric permittivity of PEDOT:PSS has been experimentally measured and fitted to the Drude–Smith model in [15].

Accordingly, the dielectric permittivity function of the Drude–Smith model with best-fitted parameters is described by

$$\varepsilon(\omega) = \varepsilon_\infty - \frac{\omega_P^2}{\omega^2 + \mathrm{i}\omega\gamma}\left(1 + c_1\frac{\gamma}{\gamma - \mathrm{i}\omega}\right), \tag{7}$$

where ε_∞, ω_P, γ, and c_1 are, respectively, the permittivity at infinite frequency, the plasma frequency, the damping rate, and the function of the carrier's initial velocity which is obtained after the collision. Here, $\varepsilon_\infty = 468$, $c_1 = -0.75$, $\omega_P/(2\pi) = 52.5$ THz, $\gamma/(2\pi) = 2.15$ THz.

2.4. Theoretical methods

The transfer matrix method (TMM) [14], which is based on the Maxwell equations, studies the propagation of an electromagnetic wave through suggested PCs by taking into account the polarization state of the incident wave and the reflection from interfaces.

For each layer, the transfer matrix is expressed by

$$M_l = \begin{pmatrix} \cos(k_{lz}d_l) & -\frac{\mathrm{i}}{p_l}\sin(k_{lz}d_l) \\ -\mathrm{i}p_l\sin(k_{lz}d_l) & \cos(k_{lz}d_l) \end{pmatrix} \tag{8}$$

where thickness of each layer is denoted by d_l. Index l labels Graphene, Si, SiO_2 or polymer. The transfer matrix M_l is determined y inserting the related parameters for the four different layers in the matrix (8). For TE polarization [14], one has

$$p_l = \frac{k_{lz}}{\omega\mu_0}, \tag{9}$$

$$k_{lz} = \sqrt{k_0^2\varepsilon_l - k_{lx}^2}, \tag{10}$$

$$k_{lx} = k_x = k_0 \sin(\theta_0). \tag{11}$$

Transfer matrix for the ideal crystal (Fig. 1a) with N periods is

$$M = (M_{\mathrm{SiO_2}} M_{\mathrm{Si}})^N = \begin{pmatrix} m_{11} & m_{12} \\ m_{21} & m_{22} \end{pmatrix}. \tag{12}$$

Similarly, for the proposed defective structure as in Fig. 1b, the transfer matrix M is given by

$$M = \begin{pmatrix} m_{11} & m_{12} \\ m_{21} & m_{22} \end{pmatrix} = \tag{13}$$

$$(M_{\mathrm{SiO_2}} M_{\mathrm{G}} M_{\mathrm{Si}} M_{\mathrm{G}})^{N_1} M_{\mathrm{P}} (M_{\mathrm{G}} M_{\mathrm{Si}} M_{\mathrm{G}} M_{\mathrm{SiO_2}})^{N_2}.$$

The reflection R can be obtained as follows [14]

$$R = |r|^2, \tag{14}$$

where

$$r = \frac{(m_{11} + m_{12} p_{n+1}) p_0 - m_{21} - m_{22} p_{n+1}}{(m_{11} + m_{12} p_{n+1}) p_0 + m_{21} + m_{22} p_{n+1}}. \tag{15}$$

For the TE polarization, one has

$$p_0 = \sqrt{\frac{\mu_0}{\varepsilon_0}} \cos(\theta_0) \tag{16}$$

and

$$p_{n+1} = \sqrt{\frac{\mu_{n+1}}{\varepsilon_{n+1}}} \cos(\theta_{n+1}), \tag{17}$$

where ε_0 and ε_{n+1} define the relative dielectric constant of the input and output planes, respectively, and θ_0 and θ_{n+1} are angles in the input and output plane, respectively.

3. Results and discussion

This section presents the numerical results of TE wave reflection properties with respect to ideal and proposed 1D photonic crystal structures. The SiO_2 and Si with permittivity $\varepsilon_{\mathrm{SiO_2}} = 3.9$ and $\varepsilon_{\mathrm{Si}} = 11.9$ are selected as dielectric layers in the crystals. With regard to the dimensional, thermal, and optical properties of graphene in this work, it was assumed that $d_{\mathrm{G}} = 0.34$ nm, $T = 300$ K, and $\Gamma = 0.11$ meV.

The PEDOT:PSS is a central defect layer with the polymer thickness of $d_{\mathrm{P}} = 500$ nm, the thickness of the Si and SiO_2 layers is considered to be 20 μm, and the period number is chosen as $N = 16$. It should be noted that the desired frequency range of 0.3–2.5 THz is dependent on the thickness of both layers and the type of polymer [15].

Figure 2 shows the reflections for the ideal crystal and the proposed crystal structure b with a polymer PEDOT:PSS defect layer without graphene.

Now, to tune the frequency of the defect mode, graphene layers are added to the structures as shown in Fig. 1b and c. It is important to note that as the number of graphene layers in the crystal structure increases, a new type of PBG appears in the low terahertz region that exhibits different properties. This new PBG region is called graphene-induced PBG (GIPBG).

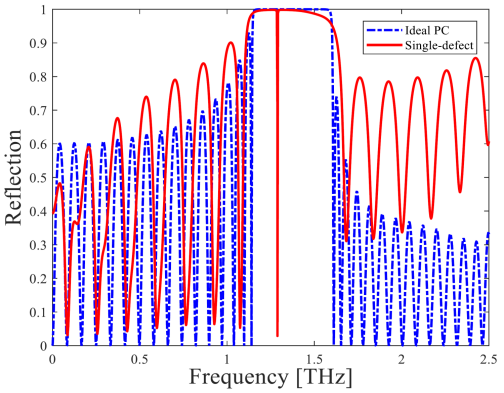

Fig. 2. Normalized reflection for an ideal and single defect polymer layer without graphene at the normal incident, $T = 300$ K, ideal PC, $N = 16$ and single defect, $N_1 = N_2 = 8$.

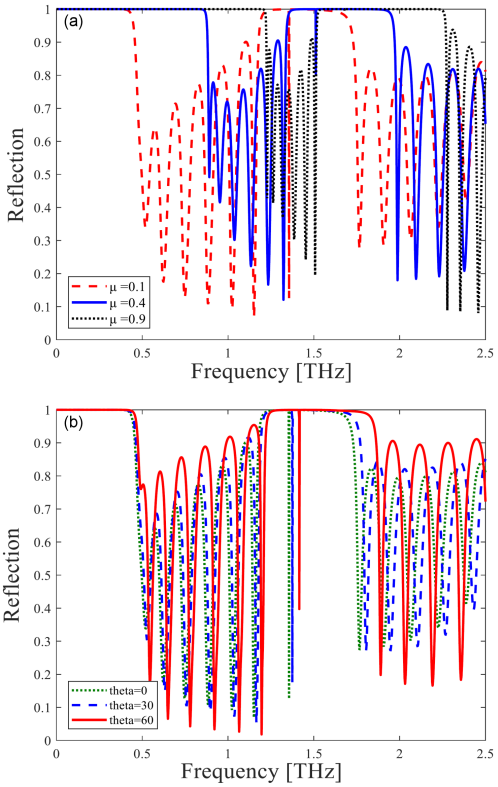

Fig. 3. Tunability of the reflection structure of $[(\mathrm{AGBG})^{N_1}]\mathrm{P}[(\mathrm{GBGA})^{N_2}]$ for (a) different graphene chemical potential for the normal incident angle and, (b) different incident angles for $\mu_c = 0.1$ eV, and physical parameters $T = 300$ K, $N_1 = N_2 = 8$.

The reflection spectrum of the proposed crystal structure b is significantly dependent on the changes in the chemical potential of graphene as displays in Fig. 3a. The GIPBG is strongly dependent on the chemical potential, and its width increases. When the graphene chemical potential grew, the

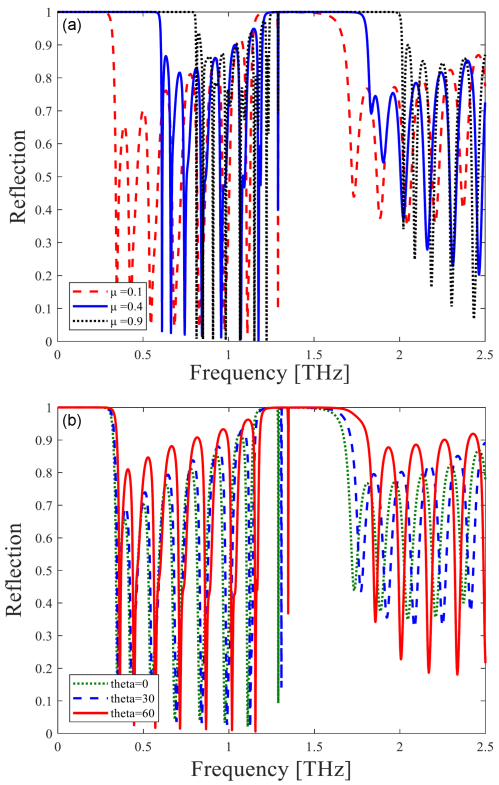

Fig. 4. Reflectance spectra of the structure $[(\mathrm{GAB})^{N_1}\mathrm{G}]\mathrm{P}[\mathrm{G}(\mathrm{BAG})^{N_2}]$ for (a) various values of graphene chemical potential for normal incident angle and (b) different angles for $\mu_c = 0.1$ eV, $T = 300$ K, $N_1 = N_2 = 8$.

left- and right-hand side limits of the PBG shift to higher frequencies, the amount of shift for the left-hand side is less than the amount of shift for right-hand side. The resonance mode slowly shifts to higher frequencies, however, its height decreases. It is noteworthy that the resonance mode disappears above $\mu = 1.0$ eV.

In the case of the structure b, the dependency of crystal reflection on the wave incidence angle is illustrated in Fig. 3b. The GIPBG is independent of the angle of incidence. By increasing the angle of the incidence wave, the width of PBG increases, and the right-hand side shift quickly to higher frequencies. Conversely, the resonance mode and the left-hand side of defect mode slowly shift to higher frequencies.

In Fig. 4a, the reflection spectrum of the structure c is plotted for different values of the chemical potentials of graphene. When the chemical potential increases, the location of the defect mode remains unchanged and only the height of the defect mode decreases. The GIPBG shifts to higher frequencies and becomes wider. The left-hand side limit of PBG shifts slightly to higher frequencies while the constant defect mode appears nearby. Conversely, the right-hand side limit of PBG shifts more quickly to the higher frequencies.

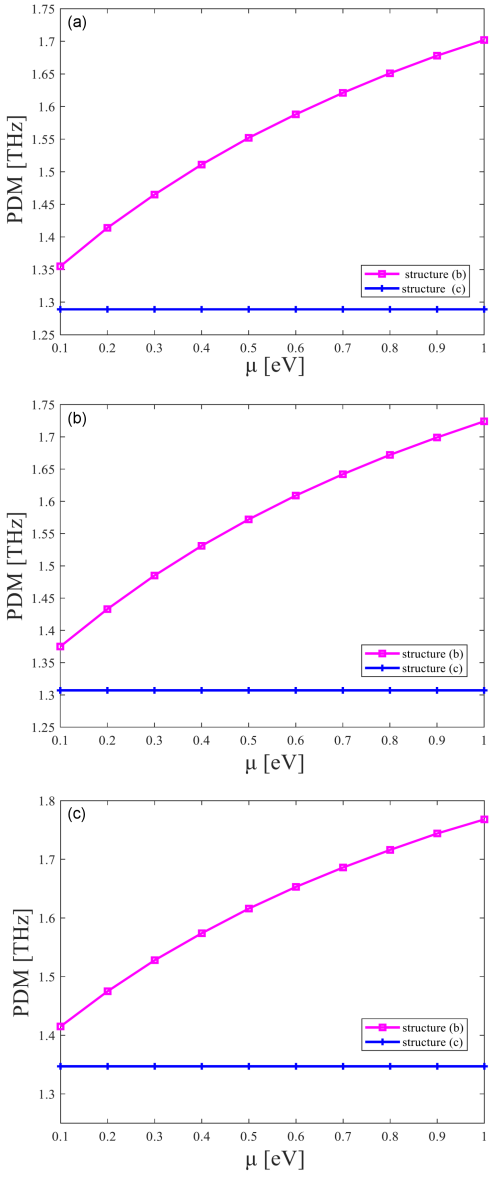

Fig. 5. The position of the reflection defect mode (PDM) in terms of different graphene chemical potentials for the incidence angles (a) $\theta = 0°$, (b) $\theta = 30°$, and (c) $\theta = 60°$.

In Fig. 4b, the effect of different angles on the reflectance spectrum of the structure c is shown. Both widths, GIPBG and PBG, have a similar enhance to those shown in Fig. 3b. By increasing the incident wave angle, the defect mode shifts to upper frequencies and its height becomes shorter.

Figure 5 shows the position of defect mode (PDM) in terms of various chemical potentials for different incidence angles $\theta = 0°$ 0, $\theta = 30°$, and $\theta = 60°$. As can be seen in Fig. 5, the position of defect mode for the structure b increases monotonically, but the position of defect mode in the structure c is a constant horizontal line for all angles. For three incidence angles, the position of the defect for the structure b is greater than the structure c.

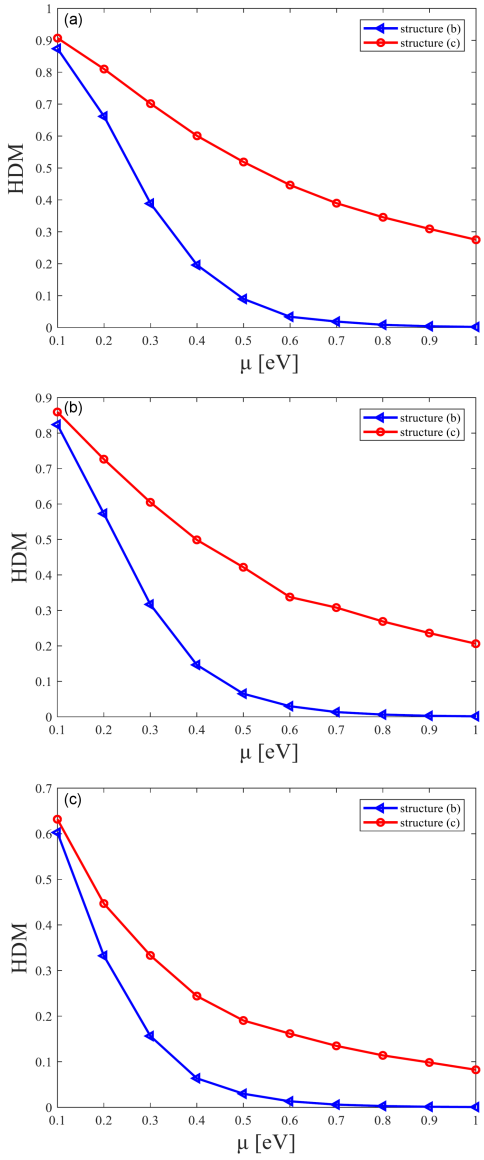

Fig. 6. The height of the defect mode (HDM) in terms of different graphene chemical potentials for the incidence angles (a) $\theta = 0^\circ$, (b) $\theta = 30^\circ$, and (c) $\theta = 60^\circ$.

The effect of the chemical potential on the height of the defect modes (HDM) for different incidence angles 0°, 30°, and 60° is shown in Fig. 6. The structure c has the greatest height of the defect mode compared to the structure b for all incidence angles. Note that both structures present a decreasing trend as the chemical potential increases.

4. Conclusions

The optical characteristics of 1D photonic crystals are investigated in detail. Using TMM, the reflection spectrum ranging from 0.3–2.5 THz is studied. An ideal photonic crystal structure containing an alternating layer of SiO_2 and Si is considered. The polymer PEDOT:PSS is inserted as a defect layer inside the proposed structures. The permittivity of PEDOT:PSS polymer is calculated by using Drude–Smith model. By adding graphene sheets to the structure, a new type of PBG, called GIPBG, emerges. Its dependency on the chemical potential of graphene is more than on the angle of the incident wave. It should be noted that when the graphene chemical potential and the wave incident angle change, the optical features of the proposed crystal structures can be tuned. By increasing the incident angle of the TE wave in the two proposed structures, the PBGs and resonance modes shift to higher frequencies. As the chemical potential increased, the PBGs width increases while the height of the defect mode decreases. The position of defect mode in the structure b shifts to higher frequencies, while for the structure c, it remains unchanged. The results obtained in this work reveal that the proposed structures can be used in the design of the tunable terahertz filters.

References

[1] E. Yablonovitch, *Phys. Rev. Lett.* **58**, 2059 (1987).

[2] S. John, *Phys. Rev. Lett.* **58**, 2486 (1987).

[3] Z. Zare, A.Gharaati, *Acta Phys. Pol. A* **125**, 36 (2014).

[4] J. Fu, W. Chen, B. Lv, *Phys. Lett. A* **380**, 1793 (2016).

[5] O. Soltani, J. Zaghdoudi, M. Kanzari, *Chin. J. Phys.* **56**, 2479 (2018).

[6] J.M. Brosi, C. Koos, L.C. Andreani, M. Waldow, J. Leuthold, W. Freude, *Opt. Express* **16**, 4177 (2008).

[7] A.H. Aly, D. Mohamed, H.A. Elsayed, D. Vigneswaran, *J. Supercond. Novel Magn.* **31**, 3453 (2018).

[8] K.V. Sreekanth, S. Zeng, K.-T. Yong, T. Yu, *Sens. Actuators B* **182**, 424 (2013).

[9] O. Soltani, S. Francoeur, Z. Baraket, M. Kanzari, *Opt. Mater.* **111**, 110690 (2021).

[10] S. Jena, R.B. Tokas, S. Thakur, D.V. Udupa, *Physica E* **126**, 114477 (2021).

[11] W. Belhadj, *Opt. Quantum Electron* **52**, 162 (2020).

[12] H. Mahmoodzadeh, B. Rezaei, *Appl. Opt.* **57**, 2172 (2018).

[13] A.A. Sayem, M.M. Rahman, M.R.C. Mahdy, I. Jahangir, M.S. Rahman, *Sci. Rep.* **6**, 25442 (2016).

[14] Y. Li, L. Qi, J. Yu, Z. Chen, Y. Yao, X. Liu, *Opt. Mater. Express* **7**, 1228 (2017).

[15] F. Yan, E.P.J. Parrott, B.S.-Y. Ung, E. Pickwell-MacPherson, *J. Phys. Chem. C* **119**, 6813 (2015).